International Journal of Bifurcation and Chaos, Vol. 10, No. 10 (2000) 2447–2463

ENCODING CARRIER AMPLITUDE MODULATIONS VIA STOCHASTIC PHASE SYNCHRONIZATION

ANDRÉ LONGTIN and MARTIN ST-HILAIRE
Département de Physique, Université d'Ottawa, 150 Louis Pasteur, Ottawa, Ontario, Canada K1N 6N5

Received November 12, 1999; Revised January 27, 2000

The firings of excitable systems can phase lock to periodic forcing. In many situations however, the firings are separated by a random number of forcing cycles, even though they occur near a preferred phase of the forcing. Also, the associated interspike interval histograms display peaks over a continuous range of integer multiples of the forcing period, and the peak heights are a unimodal function of increasing multiples of the period. This paper focusses on these patterns of stochastic phase synchronization and their alteration by physiologically relevant stimuli that modulate the amplitude of the periodic forcing. Specifically, two regimes of the FitzHugh–Nagumo system exhibiting stochastic phase locking are considered. We discuss how internal noise, originating from e.g. synaptic or conductance fluctuations, must interact with either suprathreshold or subthreshold dynamics, and in some instances with subthreshold chaos, to produce such firing patterns. These responses to constant amplitude "carriers" are then compared to those from carriers with random band-limited amplitude modulations (AM's). The comparison is based on the mean firing rate, as well as phase synchronization computed using a suitably defined input–output phase difference. Further, using the stimulus reconstruction technique to characterize synchrony between random AM's and spikes, the internal noise is shown to help transmit information about random carrier AM's in the subthreshold and slightly suprathreshold cases. This transmission also depends nonmonotonically on the carrier frequency. Our results provide biophysical insight into the dynamics of neural signal encoding that combines a mean rate code on long time scales and a precise temporal code based on phase locking on the shorter time scale of the carrier period.

1. Introduction

There has been much interest over the past two decades in the nonlinear dynamical properties of excitable systems. Studies of single cells and networks of cells have revealed such diverse properties as phase locking, chaos, bursting patterns, and a variety of collective oscillations and traveling waves. In many cases, there is also a significant "noisy" component to the underlying dynamics. This noise can interact with the aforementioned phenomena, making aperiodic an otherwise periodic firing pattern. The noise can also induce new patterns that have no deterministic counterpart.

One important aspect of the dynamics of excitable systems is the way in which they respond to variations in periodic forcing. This occurs for example when cells are stimulated by a collective oscillation of a network (to which they may or may not belong). It is particularly true for sensory neurons that must deal with oscillatory physical stimuli such as pure sound tones and other vibrations (see e.g. [Rose *et al.*, 1967]), or electric fields [Zakon, 1986]. In those cases, it is often the modulations of the "carrier" oscillation that convey an important part of the relevant signal. Such modulations usually occur on a slower time scale than the period of the carrier itself.

It is an interesting question to ask how carrier amplitude modulations (AM's) are converted to "spike trains" or sequences of "action potentials" or "firings", the output of excitable systems. What are the phase locking properties of the spikes to the carrier, how are they modified by the AM's and by sources of internal noise in the cell?

One popular approach to this problem is the "black box" transfer function, where one characterizes the linear properties of the cell in the frequency domain (see e.g. [Nelson *et al.*, 1997]). Another approach is based on modulated point processes, wherein the dynamical equations that lead to spikes are inaccessible, and the cell is characterized by the statistics of a spike generator which generates spikes randomly but at a rate dependent on the input [Johnson, 1996]. A more recent approach, relevant in the context of randomly varying signals, is the stimulus reconstruction technique ([Rieke *et al.*, 1997], see Sec. 2). This technique calculates, using the stimulus and the output spike train, an optimal filter which, when convolved with the spike train, creates a linear estimate of the stimulus. This approach allows the computation of signal-to-noise ratios and information transfer rates from stimulus to spike train.

The transfer function approach can take into account the often present noisy fluctuations of the responses to repeated deterministic input, e.g. by averaging the firing rate over some temporal window before comparing the gain and phase of this averaged waveform to those of the input. The point process approach in fact takes the intrinsic variability in spike times of the cell, due to internal noise or synaptic input [Segundo *et al.*, 1994], as its starting point. The reconstruction technique does not make any assumptions about the internal dynamics of the cell, as long as the input is a stochastic process.

On the other hand, much is also known about deterministic phase locking in periodically forced excitable or autonomously oscillating systems (see e.g. [Rescigno *et al.*, 1970; Glass & Mackey, 1988; Gerstner *et al.*, 1996; Pikovsky *et al.*, 1997]). There has also been much recent interest on the effect of noise on phase locking and signal transduction in such systems [Gammaitoni *et al.*, 1998; Lewis & Henry, 1995; Kurrer & Schulten, 1995; Longtin, 1993; Motz & Rattay, 1986]. This is relevant, given that often noise is either present in the cell (e.g. channel conductance fluctuations), or arises from the random component of synaptic release and reuptake mechanisms, or is a manifestation of chaotic behavior at the single cell or network level.

In this paper, we focus on two dynamical mechanisms that produce stochastic phase synchronization to a carrier, and study how these mechanisms are altered by amplitude modulations of the carrier. We consider the FitzHugh–Nagumo system as a generic excitable system, and the two mechanisms refer to supra- and subthreshold regimes of this system (defined below). This system is generic in the sense that it captures many features of the firing dynamics of so-called type II membrane dynamics. For these, the frequency of action potentials is nonzero at the onset (via a Hopf bifurcation) of autonomous oscillation; this onset results from a change in the bias parameter in the current balance equation. Results on type I dynamics, associated with saddle-node bifurcations, are forthcoming. We note here that the FHN model differs from the often-studied integrate-and-fire-type models, mainly because it has a deterministic resonance and a built-in refractory period. It has also been used in recent studies of firing variability in excitable systems [Brown *et al.*, 1999; Lindner & Schimansky-Geier, 1999; Pikovsky *et al.*, 1997; Collins *et al.*, 1995; Longtin, 1993; Treutlein & Schulten, 1985; Clay, 1976]. It thus serves as a starting point to investigate more detailed excitable cell models, especially as in many circumstances, such details are not available due to the unavailability of intracellular potential measurements.

We expect that our study is relevant to the processing of amplitude modulations in many receptors, such as auditory and mechanoreceptors [Rose *et al.*, 1967]. The shape of the interspike interval histograms (ISIH) generated by the FHN model in the regimes studied below belongs to the class of gamma-type distributions, which have a unimodal envelope and an exponential decay at long intervals. Because of this, our analysis is relevant only to a subset of electroreceptors of weakly electric fish. The probability of firing per carrier cycle of so-called P-units encodes amplitude modulations of the carrier; this carrier, which oscillates as high as 900 Hz in certain species, is generated by the fish; environmental stimuli generate band-limited AM's. Our results would be relevant to the subset of those receptors which possess gamma-type (rather than approximately Gaussian) ISIH's, i.e. to those which have a high-probability of firing per carrier cycle [Zakon, 1986; Wessel *et al.*, 1996].

In the first part of the paper, we consider the problem of obtaining smooth ISIH's from the FHN model in the excitable regime in the presence of constant amplitude (1) subthreshold and (2) suprathreshold sinusoidal forcing. We also discuss the so-called "subthreshold chaos" regime, and characterize phase synchronization as a function of noise. The second part of the paper considers the encoding of time varying signals into spike trains in both the subthreshold and suprathreshold regimes, with the associated modification of phase synchronization properties. We confine our study to the vicinity of threshold, specifically on carriers that are slightly below and slightly above threshold. This is because many neural systems, especially at the sensory periphery, adapt their threshold over time so that incoming signals lie in the vicinity of threshold (see e.g. [Xu *et al.*, 1996]). Note that, in the context of amplitude modulations, the model studied here has two distinct and uncorrelated stochastic forcing terms: One for the input amplitude modulations, and the other for the internal noise in the cell (mainly synaptic noise and conductance fluctuations).

The outline of the paper is as follows. In Sec. 2, we present the dynamical equations of interest, and describe the numerical integration and the stimulus reconstruction technique. Section 3 examines how noise enables the production of the smooth multimodal ISIH's seen experimentally in response to deterministic periodic forcing, using the FitzHugh–Nagumo model in both the subthreshold and suprathreshold regimes. It also studies phase synchronization properties of these regimes as a function of internal noise, using ISIH's, mean firing rates and input–output phase difference behavior. Section 4 considers the effect of random amplitude modulations on the stochastic phase locking in the subthreshold regime. Section 5 considers the effect of random AM's in the suprathreshold regime. In both Secs. 4 and 5, ISIH's are presented along with firing rate and phase difference behavior, since the spikes still exhibit phase synchronization to the carrier on a short time scale. However, we show how this phase locked firing allows a "representation" of the random stimulus that evolves on a slower time scale, and study how this representation depends on the intensity of the internal noise. We will show that the internal noise helps the encoding of AM's in the subthreshold case, a consequence of stochastic resonance exhibited by this model. This is similar to stochastic resonance with random signals [Collins *et al.*, 1995; Levin & Miller, 1996], except for the presence of a carrier which maintains, by virtue of the phase synchronization, a temporal neural code rather than only a mean rate code [Theunissen & Miller, 1995]. This temporal code is maintained below and above-threshold in our model study. The paper ends with a discussion in Sec. 6.

2. Methods

2.1. *Dynamical equations*

We consider the FHN model with sinusoidal forcing and additive noise, as in [Longtin, 1993], as well as random amplitude modulations, introduced in [Longtin, 2000]

$$\varepsilon\frac{dv}{dt} = v(v-a)(1-v) - \omega + r[1+s(t)]\sin\Omega t + I + \eta_1(t) \quad (1)$$

$$\frac{d\omega}{dt} = v - d\omega - b \quad (2)$$

$$\frac{d\eta_1}{dt} = -\lambda_1\eta_1 + \lambda_1\xi_1(t) \quad (3)$$

$$\frac{ds}{dt} = z_1 \quad (4)$$

$$\frac{dz_1}{dt} = z_2 \quad (5)$$

$$\frac{dz_2}{dt} = z_3 \quad (6)$$

$$\frac{dz_3}{dt} = -4\alpha z_3 - 6\alpha^2 z_2 - 4\alpha^3 z_1 - \alpha^4 s(t) + \eta_2(t) \quad (7)$$

The frequency is $\Omega = 2\pi/T$. The fast membrane potential dynamics $dv(t)/dt$ are driven by two independent zero-mean noise sources. The Gaussian stochastic process $s(t)$ used to mimick amplitude modulations of the carrier is obtained by lowpass filtering Ornstein–Uhlenbeck noise $\eta_2(t)$ from a second independent source. The response function of this filter is chosen as $H(\Omega) = \alpha^4/(j\Omega+\alpha)^4$. This filter with a fourth-order pole closely approximates that used to create band-limited carrier fluctuations in [Wessel *et al.*, 1996]. Here we use the same basic FHN parameters as in previous work [Collins *et al.*, 1995; Chialvo *et al.*, 1997], namely $a = 0.5$, $b = 0.15$, $d = 1$, $I = 0.04$, and $\varepsilon = 0.005$. We also

set the cutoff frequency at $\alpha = 0.5$. The amplitude modulations represent realistic signals to be encoded by the excitable system. The term $s(t)$ appears at first glance to be a multiplicative noise; however, its intensity is independent of the state variables, so it is in fact additive noise. Nevertheless, it is multiplied by the mean carrier amplitude r.

The noise $\eta_2(t)$ used here is actually an OU process with adjustable correlation time λ_2^{-1} and variance $D_2\lambda_2$. Gaussian white noise would have suited our purpose here as well. For all simulations presented below, this correlation time is 0.001 s, much shorter than the inverse of the bandwidth of the filter $H(\Omega)$. A value of $D_2 = 0.2$ yields AM's with a standard deviation of 15%, which is physiologically realistic (see e.g. [Wessel *et al.*, 1996]).

The internal noise $\eta_1(t)$ may come from many sources. For example, a primary sensory neuron is generally composed of a receptor cell, that transduces a physical stimulus into a voltage, plus nerve endings that connect to this receptor to higher brain structures. The receptor releases a chemical ("neurotransmitter") onto these nerve endings. This is usually described as a stochastic release mechanism that is modulated by the receptor potential. The fluctuations produced at this level, along with conductance fluctuations in the cell, can be lumped together in a first approximation as an "internal" noise source. This band-limited internal noise fluctuates on a time scale commensurate with or faster than those associated with neural spiking. We model it here as additive OU noise on the fast voltage variable, with correlation time $\lambda_1^{-1} = 0.001$ and variance $D_1\lambda_1$.

One issue that will be considered below is the effect of this internal noise on neural firings that are phase synchronized to the carrier; another is its effect on the information about the random signal (i.e. about random amplitude modulations caused by objects in the environment) that is conveyed by the output spike train.

For all our simulations with amplitude modulation, we have chosen $D_2 = 0.2$, which yields AM's with standard deviation ≈ 0.15. The internal noise parameter D_1, which will be varied in our study, will hereafter be denoted by D for simplicity. Numerical integration of this stochastic model is as in [Longtin, 1993] (an order-1 algorithm) with an integration time step of 0.001. As the FHN system is a reduced description of a conductance-based model, some of its parameters do not have straightforward biophysical interpretations; nevertheless, the lumped effect of different noise sources can, to a first approximation, be studied via the additive dynamical noise used in Eq. (7) (see also [Tuckwell & Rodriguez, 1998] and references therein).

2.2. *Quantifying the information transfer*

There are two aspects of phase synchronization that can be investigated in the presence of amplitude modulations of the sinusoidal forcing. The first aspect concerns the effect of the AM's on the synchronization between the firings and the modulated carrier itself, as well as on the mean firing rate. The second aspect concerns how well the firings are synchronized to the fluctuations that make up the AM itself, and which are the important relevant signals. We address the first question by recomputing the behavior of the mean firing rate and input–output phase difference in the presence of the AM, and this, for varying amounts of internal noise. As for the second question, we use an information theoretic measure of synchrony between spikes and AM's [Wessel *et al.*, 1996; Rieke *et al.*, 1997]. We adopt this scheme because it is becoming one standard tool of spike train analysis in the neurosciences. Also, since the AM's are manifestations of a band-limited noise, the notion of phase is not the most natural for it, even though a phase could be extracted from such a signal using the Hilbert transform (i.e. analytic signal techniques). We note that the more common definition of phase based on the angle of the phase point in a two-dimensional phase space (such as $x_3(t)$ versus $x_4(t)$) leads to phase ambiguities, as revolutions do not always encircle the origin.

We use the stimulus reconstruction technique in the implementation of [Wessel *et al.*, 1996]. The goal of this algorithm is to find a response filter $h(t)$ which, when convolved with the spike train, gives a "reconstructed stimulus" that is closest, in the least squares sense, to the original stimulus that elicited the spike train. In the context of our study, the stimulus to be reconstructed is only the amplitude modulation. Let $s(t)$ be the input to the neuron [corresponding to $s(t)$ in Eq. (7)]. We then define the zero-mean spike train:

$$x(t) = \sum_i \delta(t - t_i) - \overline{x(t)} \tag{8}$$

where $\overline{x(t)}$ is the temporal average of the sum of

delta functions over one realization, and t_i are the spike times. A linear estimate of $s(t)$ is given by

$$s_{\text{est}} = \int_0^T dt' h(t-t')x(t') \,. \tag{9}$$

The reconstruction filter is chosen to minimize the mean square error ε,

$$\varepsilon^2 = \frac{1}{T}\int_0^T dt[s(t) - s_{\text{est}}(t)]^2 \,. \tag{10}$$

It is given by [Wessel *et al.*, 1996]

$$h(t) = \int_{-f_c}^{f_c} df \frac{S_{sx}(-f)}{S_{xx}(f)} \exp^{-2\pi i f t} \tag{11}$$

where f_c is the cutoff frequency of the filter $H(\omega)$, and S_{xx} and S_{sx} are, respectively, the auto-spectrum of the output spike train and the cross-spectrum of the input signal and spike train. Once this filter $h(t)$ has been estimated, it is convolved with the whole spike train to yield an "estimated signal" or "reconstructed signal" s_{est}. The difference between the real input and s_{est} is known in that method as the "noise" in the system; it does not have a direct biophysical interpretation; it is in fact "reconstruction noise" and depends on system properties and those of the input and internal noises. This noise is:

$$n(t) = s_{\text{est}}(t) - s(t) \tag{12}$$

The mean square error is then:

$$\varepsilon = \left[\int_{-f_c}^{f_c} df\, S_{nn}(f)\right]^{1/2} \tag{13}$$

where S_{nn} is the auto-spectrum of the reconstruction noise. The coding fraction is finally defined as

$$\gamma = 1 - \frac{\varepsilon}{\sigma} \tag{14}$$

where σ is the standard deviation of the AM signal. A coding fraction of 1 is the best possible (linear) coding of the signal into the spike train; $\gamma = 0$ is the worst coding, where the mean square error is on average equal to σ.

3. "Smooth Skipping" from Periodic Forcing

In this section, only sinusoidal forcing with constant amplitude r is considered; this corresponds to $s(t) = 0$ in Eq. (7). We begin by making a clear distinction between the subthreshold and suprathreshold regimes referred to throughout this paper. The distinction relies on the deterministic properties of the model, i.e. on its properties in the absence of stochastic forcing. The model is said to be in the subthreshold regime if, in the presence of sinusoidal forcing, it does not generate spikes in the asymptotic regime (although it may generate one or more spikes during a short transient evolving from the initial condition). Otherwise, it is in the suprathreshold regime.

Different neuron models have different types of phase space boundaries which determine whether or not a spike occurs. Certain models have a true threshold, and spikes are an all-or-nothing event, while others have a pseudo-threshold, and the spike size is a continuous, although usually steep function of stimulus amplitude. The FHN model studied here admits such graded spike responses [Clay, 1976]. Also, in the presence of stochastic forcing on the dynamical variables, as occurs in the real system, there is always a finite probability that a noise-induced spike could occur, regardless of the threshold type. We choose a minimal value of spike size (0.5 in the models' units); a positive-going excursion of the fast voltage variable that reaches beyond this value, and which is separated from the previous spike by at least the absolute refractory period (corresponding to the width of spike, i.e. ≈ 0.4 s in the model's units) is considered here as a spike.

3.1. *Deterministic case*

Sinusoidal forcing in the subthreshold regime produces no spikes in the steady state. In contrast, spikes occur periodically in the suprathreshold regime. For the suprathreshold case of concern in our paper, the resulting pattern is actually 2:1 firing, i.e. one spike for every two forcing cycles. This pattern is visible in one spiking portion of Fig. 5B. The precise firing pattern depends on the Arnold tongue structure of the system [Longtin & Chialvo, 1998; Longtin, 2000]. Another effect which also underlies the Arnold tongue structure is the fact that the amplitude of the voltage response to sinusoidal input depends on the frequency of this sinusoid, via the deterministic resonance of the FHN oscillator [Longtin, 2000]. In particular, for the parameters of our study, the forcing frequency is very close to the deterministic resonance of the FHN model, i.e. to the frequency which requires the least amplitude to

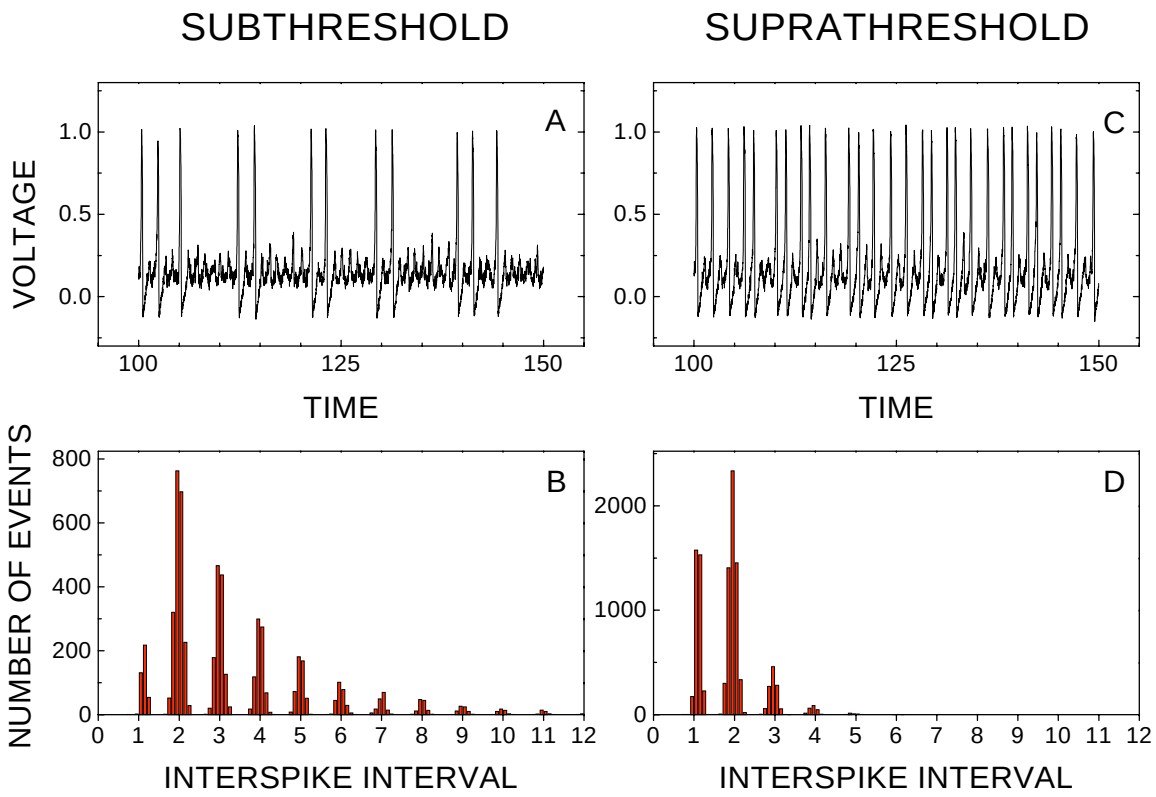

Fig. 1. Voltage time series and interspike interval histograms (ISIH) from the numerical integration of Eq. (7) with a fixed time step of 0.001, in the absence of random amplitude modulation. (A) Voltage for the subthreshold regime ($r = 0.01$) with $D = D_1 = 5 \times 10^{-7}$. (B) ISIH corresponding to the parameters in (A). (C) Same as in (A) except that the sinusoidal forcing is suprathreshold ($r = 0.014$). (D) ISIH corresponding to the parameters in (C). ISIH's are constructed using 200 bins, and by accumulating ISI's from a single realization that generated 10 000 spikes. The EOD forcing frequency is $\Omega/(2\pi) = 1$ Hz in the scaled units of this model. Time can be scaled appropriately to mimick a real EOD frequency around 800 Hz. In these units, the absolute refractory period is ≈ 0.4 s, which can correspond to a few milliseconds in a typical case. A spike is counted only if it occurs at least 0.4 s after the previous spike.

produce 1:1 firing. It is known that, for certain senses that encode time-varying stimuli using a periodic carrier, a carrier frequency close to the resonance of the receptor is often used [Zakon, 1986].

There is also another regime which has been investigated in the noiseless case in [Longtin, 1993; Kaplan *et al.*, 1996; Clay & Shrier, 1999]. Certain combinations of frequency and amplitude of forcing lead to chaotic spiking that shows phase preference; in other words, spikes occur always near a preferred phase of the forcing, but not at every cycle. This is the kind of firing pattern that concerns us in this paper; we will be especially concerned with its alteration by random amplitude modulations. In [Longtin, 1993], such chaotic "skipping" occurs with sinusoidal forcing. In [Kaplan *et al.*, 1996; Clay & Shrier, 1999], it is obtained by forcing with periodically repeating rectangular pulses. The latter paper describes the resulting firing pattern as "subthreshold chaos", although clearly, this "subthreshold" chaos can produce "suprathreshold" responses (spikes). The interspike interval histograms produced by this chaotic spiking have peaks near integer multiples of the driving period.

However, the "chaotic" ISIH's typically lack peaks at certain integers, and one can often see finer structure within these peaks due to the chaotic dynamics [Longtin, 1993; Kaplan *et al.*, 1996; Clay & Shrier, 1999]. Interesting as they are, those kinds of chaotic patterns do not have the smooth peaks and continuous sequence of peaks are seen in many senses, such as those for auditory neurons [Rose *et al.*, 1967] which are very similar to those presented in Fig. 1.

3.2. *Stochastic case*

The addition of dynamical noise to such chaotic skipping models washes out the finer structure within ISIH peaks, yields a sequence of peaks over

a contiguous range of multiples of the driving period [Longtin, 1998], and the envelope of the peaks is unimodal — all characteristics of histograms seen e.g. in auditory physiology. This suggests that, if subthreshold chaos underlies such firing patterns, then it must be accompanied by a significant amount of noise; a likely origin for this noise is the synaptic noise onto the afferent nerve fiber that innervates the receptor cell.

In this paper, we focus on the firing patterns for sinusoidal stimuli in the vicinity of threshold. It is known that many cells adapt their threshold in order that the signals of interest are in the vicinity of this threshold (see e.g. [Xu *et al.*, 1996] and references therein). We consider first the effect of internal noise on the response to subthreshold and suprathreshold sinusoidal forcing (Fig. 1). The only difference between Figs. 1A and 1B is the carrier amplitude and the sequence of internal noise values. Without noise, there would be no spikes in Fig. 1A, and there would be a periodic 2:1 pattern in Fig. 1B. These results are known from previous studies (see e.g. [Longtin, 1993]), and are meant here to set the stage for studying the effect of amplitude modulations. They are also shown because we will investigate phase synchronization in the context of these skipping patterns.

We note that the mean firing rate follows an Arrhenius law $\langle f \rangle \sim \exp(-U/D)$ except at higher noise levels; here U is an effective barrier height [Longtin, 2000]. The suprathreshold case corresponds to a lower barrier, thus to a smaller mean

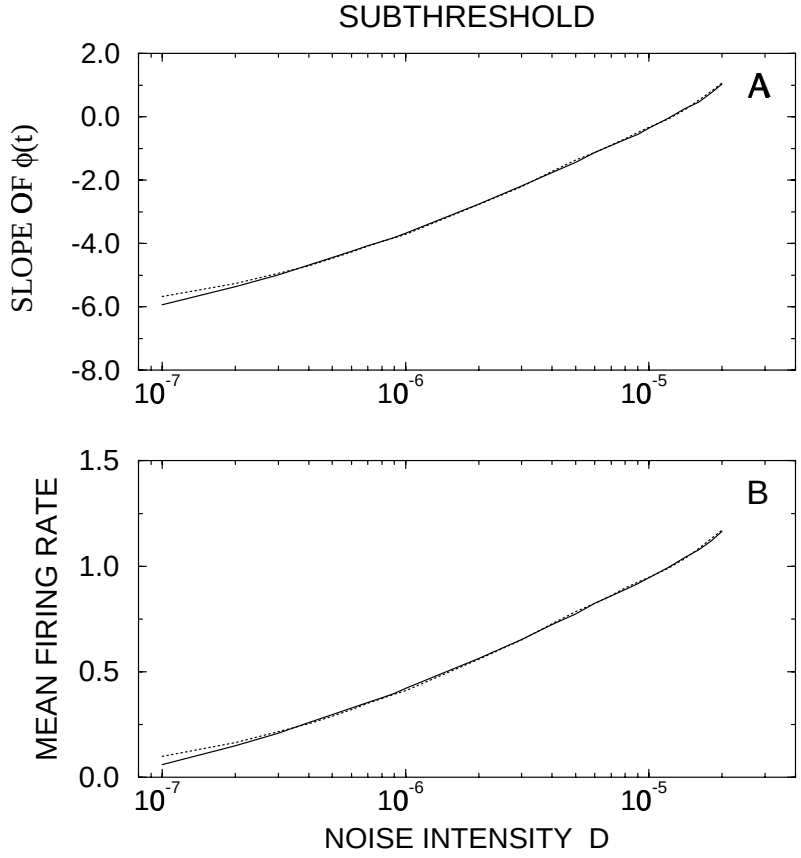

Fig. 2. Phase synchronization in the subthreshold regime ($r = 0.01$) for increasing internal noise intensities $D = D_1$. The stimulus frequency is $f = 1$ Hz in each case. (A) The phase difference $\phi(t)$ [Eq. (16)] between the system response and the input follows an approximately linear time course; the slope of this relationship, which corresponds to a mean frequency, is plotted for different values of D. Twenty five realizations of 2×10^5 integration time steps were used to compute an ensemble average of $\phi(t)$, from which the slope was estimated by linear regression. The solid (dotted) curve is for simulations without (with) random carrier amplitude modulations (15%). Note that only the internal noise values differed across realizations. In all cases, the linear correlation coefficients are close to 1.0 except for the case where the slope of $\phi(t)$ is near zero. (B) Mean firing rate versus internal noise intensity, obtained from the same realizations that provided the data in (A). Results are shown for the subthreshold regime without (solid line) and with (dotted line) amplitude modulations.

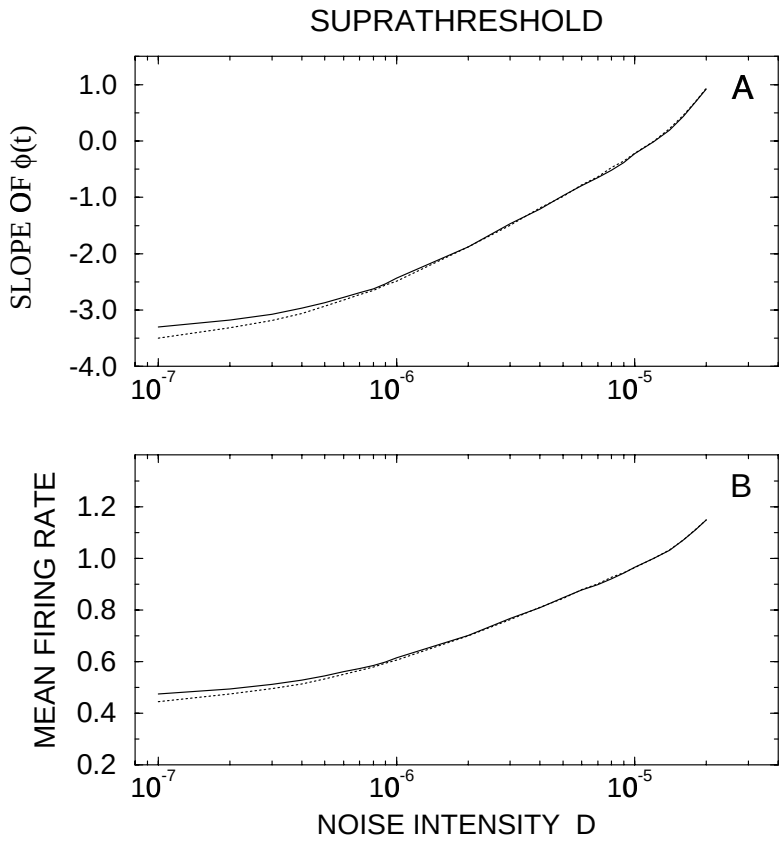

Fig. 3. Same as in Fig. 2, except that the regime here is suprathreshold ($r = 0.014$). (A) Slope of the time course of the phase difference for different noise intensities, without (solid) and with (dotted) amplitude modulations. (B) Same as in Fig. 2B, but for the suprathreshold regime. The EOD carrier frequency is 1 Hz.

ISI or larger mean firing rate (the reciprocal of the mean ISI). This mean rate is plotted versus the internal noise D in Figs. 2B and 3B (solid curves).

3.3. *Phase synchronization*

Let the phase of the input signal at the time of a spike be

$$\psi_{\rm in} = 2\pi t_i/T + \phi_o \qquad (15)$$

where ϕ_o is the initial phase of the forcing, and T the forcing period. We can also associate a phase to the output of the neuron, as in [Neiman *et al.*, 1999]: we simply increment the output phase $\psi_{\rm out}$ by 2π whenever a spike occurs; this corresponds to a "loop" in the phase space of the excitable system. The output phase is thus $\phi_{\rm out}(t_i) = 2\pi i + \phi_o$, where i corresponds to the number of spikes that have occurred up to time t_i (it is the same index as in t_i below). While the input phase increases at a constant rate for sinusoidal forcing, the output phase behaves as a birth process, where the time intervals between "births" are distributed according to the ISIH. Given that the intervals are not distributed exponentially, as for a Poisson process, this is not a standard birth process. We verified however that the intervals have negligible serial correlations, and thus the ISI's (i.e. the renewal process) extracted from this birth process are independent, as for a Poisson process.

We can then define the phase difference

$$\phi(t) \equiv \psi_{\rm out} - \psi_{\rm in}\,. \qquad (16)$$

Figure 2A shows the behavior of this relative phase as a function of time for the subthreshold case, and Fig. 3A for the suprathreshold case. This relative phase evolves linearly in time at a rate that depends on the internal noise intensity. Thus, we have plotted this rate, which corresponds to a relative angular frequency between system and input, as a function of D, both without and with amplitude modulations. We see that the slope increases monotonically past zero. When the phase difference is zero, one can say that the input and output are synchronized. However, due to the lack of a plateau,

i.e. of a range of D over which the mean relative frequency is constant, one cannot stricly speak of nonlinear synchronization here. Other quantities such as the effective phase diffusion [Neiman *et al.*, 1999] may reveal such synchronization, and will be investigated elsewhere.

3.4. *Simple statistical model*

A simple statistical model of the spiking reveals that this definition of phase difference is directly related to the mean firing rate, even though the two quantities are computed differently. This would explain the similarity between the two curves, in both the sub- and suprathreshold cases, since the model does not distinguish between these cases. Because of its nondynamical nature, the model is also not expected to yield information on nonlinear phenomenon such as phase locking regions. Let $\{t_i\}$ be a sequence of firing times. We can write $t_i = n_i T + \xi_i$ where n_i is a random integer variable that increases monotonically with the index i, and ξ a continuous random variable; ξ_i is Gaussian to a good approximation, since it describes the jitter in the phase locking. The intervals τ_i can then be written

$$\mathrm{ISI}_i = t_i - t_{i-1} \equiv m_i T + \xi_i - \xi_{i-1} \qquad (17)$$

where $m_i \equiv n_i - n_{i-1}$. The quantity m_i corresponds to the nearest integer number of forcing periods corresponding to ISI_i. Its distribution $P(m)$, which corresponds to the envelope of the ISIH, follows typically a gamma distribution (see Fig. 1). We assume that both m_i and ξ_i are independent and identically distributed random variables. As D increases, we know from our simulations of the FHN system that the mean of $P(m)$ decreases, while the variance of ξ increases. The phase difference is

$$\phi(t_i) = 2\pi i - \frac{2\pi}{T}(n_i T + \xi_i)\,. \qquad (18)$$

The average of this phase difference at the time t_i of the ith spike is

$$\langle \phi(t_i) \rangle = 2\pi(\langle i \rangle - \langle n_i \rangle)\,. \qquad (19)$$

On the other hand we have $\langle \mathrm{ISI} \rangle = \langle m \rangle T$, where $\langle m \rangle$ is the mean of $P(m)$. Since $\langle n_i \rangle$ is the average number of forcing cycles that have elapsed at the time of the ith spike, we have $\langle i \rangle = \langle n_i \rangle / \langle m \rangle$. Thus, we have

$$\langle \phi(t_i) \rangle = 2\pi \langle n_i \rangle [T\langle R \rangle - 1] \qquad (20)$$

where $\langle \mathrm{ISI} \rangle^{-1} = \langle R \rangle$, the mean firing rate. Finally, since $\langle t_i \rangle = \langle n_i \rangle T$, we have the slope

$$\frac{d\langle \phi(t_i) \rangle}{d\langle t_i \rangle} = 2\pi \left(\langle R \rangle - \frac{1}{T} \right)\,. \qquad (21)$$

We thus see that the mean firing rate and the slope of the phase difference are proportional to one another. In particular, this slope is zero when the mean firing rate is the reciprocal of the forcing period T; this is clearly seen in Figs. 2 and 3.

4. Coding AM's from the Subthreshold Regime

4.1. *Deterministic case*

Figure 4B shows the voltage response of the FHN model to an amplitude-modulated input in the absence of internal noise for the subthreshold case. Spiking occurs only rarely on the occasional large positive fluctuations of the Gaussian AM (none are

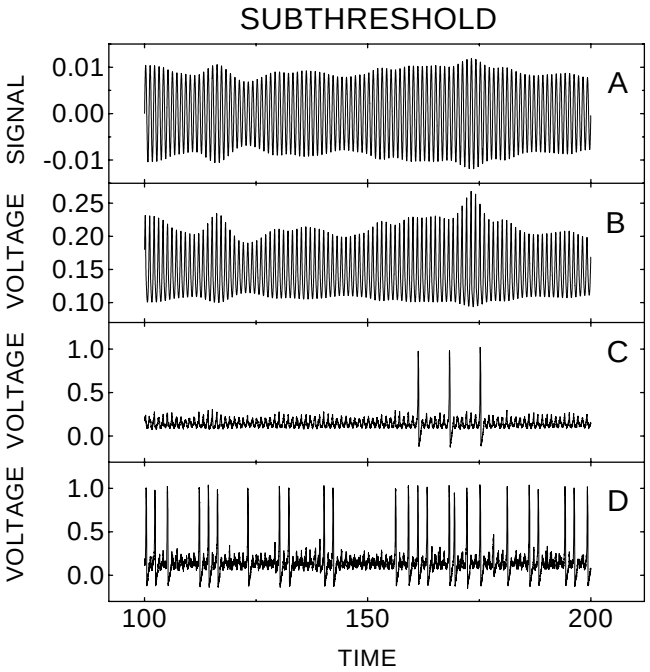

Fig. 4. Encoding of amplitude modulations in the subthreshold regime ($r = 0.01$). The OU process that drives the low pass filter is characterized by $D_2 = 0.2$ and $\lambda_2 = 0.001$, yielding a stochastic AM with standard deviation equal to 0.18. This is referred to as an 18% modulation of the carrier. (A) Amplitude modulated carrier signal is the input to the FHN model as in Eqs. (1)–(7). Other panels represent the membrane potential versus time for different noise internal intensities D: (B) 0, (C) 10^{-7} and (D) 5×10^{-7}. The EOD carrier frequency is 1 Hz.

seen in Fig. 4B). The magnitude of the voltage response to the AM's depends on the frequency of the carrier. If this frequency is near the resonance frequency of the FHN model, as is the case for $T = 1$, the AM's also have a large magnitude. Thus, the tuning characteristics of the FHN model with respect to carrier frequency [Hochmair-Desoyer *et al.*, 1984; Longtin, 2000] will directly impinge on the ability of the model to generate spikes in response to the AM's. This effect will be studied in Sec. 4.3 (see Fig. 10).

4.2. *Stochastic case*

The effect of internal noise on the firing patterns is shown in Figs. 4C and 4D. The internal noise increases the probability of firing in response to positive fluctuations of the voltage. As Fig. 6 shows, the effect of D on the ISIH is thus to produce shorter intervals, both in the absence and presence of AM's. The AM's increase the mean firing rate, even though they are zero-mean fluctuations. This is because the AM's carry the system near and above threshold, increasing the firing probability per forcing cycle proportional to the instantaneous AM height. In turn, the positive curvature of the sigmoidal firing characteristics, i.e. a plot (not shown) of the mean firing rate-versus-bias current I in Eq. (1) (see [Chialvo *et al.*, 1997]) underlies the fact that the AM here creates more spikes than it deletes. This is further substantiated in Fig. 2 where it is seen that the effect of the AM (dotted line) is to increase the mean firing rate, and consequently, the slope of $\phi(t)$. The effect of the AM is negligible at higher D, as the dominant effect on the increase of the firing rate is D itself; the variance of the AM becomes relatively smaller than the noise fluctuations produced by the internal noise.

4.3. *Coding fraction*

The AM's elicit a pattern of spikes in which the mean spiking frequency, averaged over a few carrier cycles, follows the band-limited AM's. This is clear from Fig. 4. This is a consequence of the linearization of the abrupt threshold, i.e. of the firing rate versus input curve [Chialvo *et al.*, 1997]. In other words, because of the noise, an increase in input signal (such as in the mean bias parameter I in Eq. (1)) produces a proportional increase in firing rate, even in the range of the AM fluctuations where no spikes are elicited.

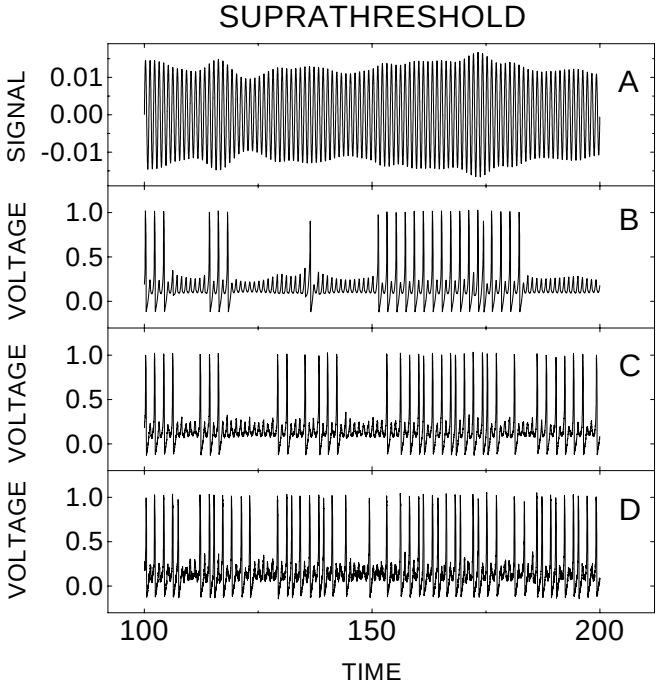

Fig. 5. Encoding of amplitude modulations (see Fig. 4) in the suprathreshold regime ($r = 0.014$). (A) Input signal. Internal noise intensities D are: (B) 0, (C) 10^{-7} and (D) 5×10^{-7}. The EOD carrier frequency is 1 Hz.

Figures 8 and 9 study the coding fraction as a function of internal noise D for different values of the mean carrier amplitude r [Eq. (1)]. Note that the variance of the AM's which drive the voltage dynamics effectively increase with r because of the multiplication $rs(t)$ in Eq. (1). These are called "constant contrast" simulations, i.e. the ratio of AM variance to carrier mean amplitude is constant throughout our work.

We first note that, for all r values considered, the coding fraction is greater than zero. This is true even though the unmodulated EOD is subthreshold for $r < 12.8$, and is due to the random nature of the AM: Certain fluctuations of the AM go above threshold, and thus are encoded even without internal noise (i.e. even with $D = 0$).

Also, in this subthreshold regime, increasing D first increases the coding fraction, i.e. the quality of the encoding (Figs. 8 and 9). In this region, greater internal noise such as synaptic noise raises the firing rate; this amounts to a higher sampling of the underlying AM waveform, thus improving information transfer. This is true even though most of the dynamic range of the AM fluctuation is subthreshold, a consequence of the aforementioned linearization. The coding fraction then goes through

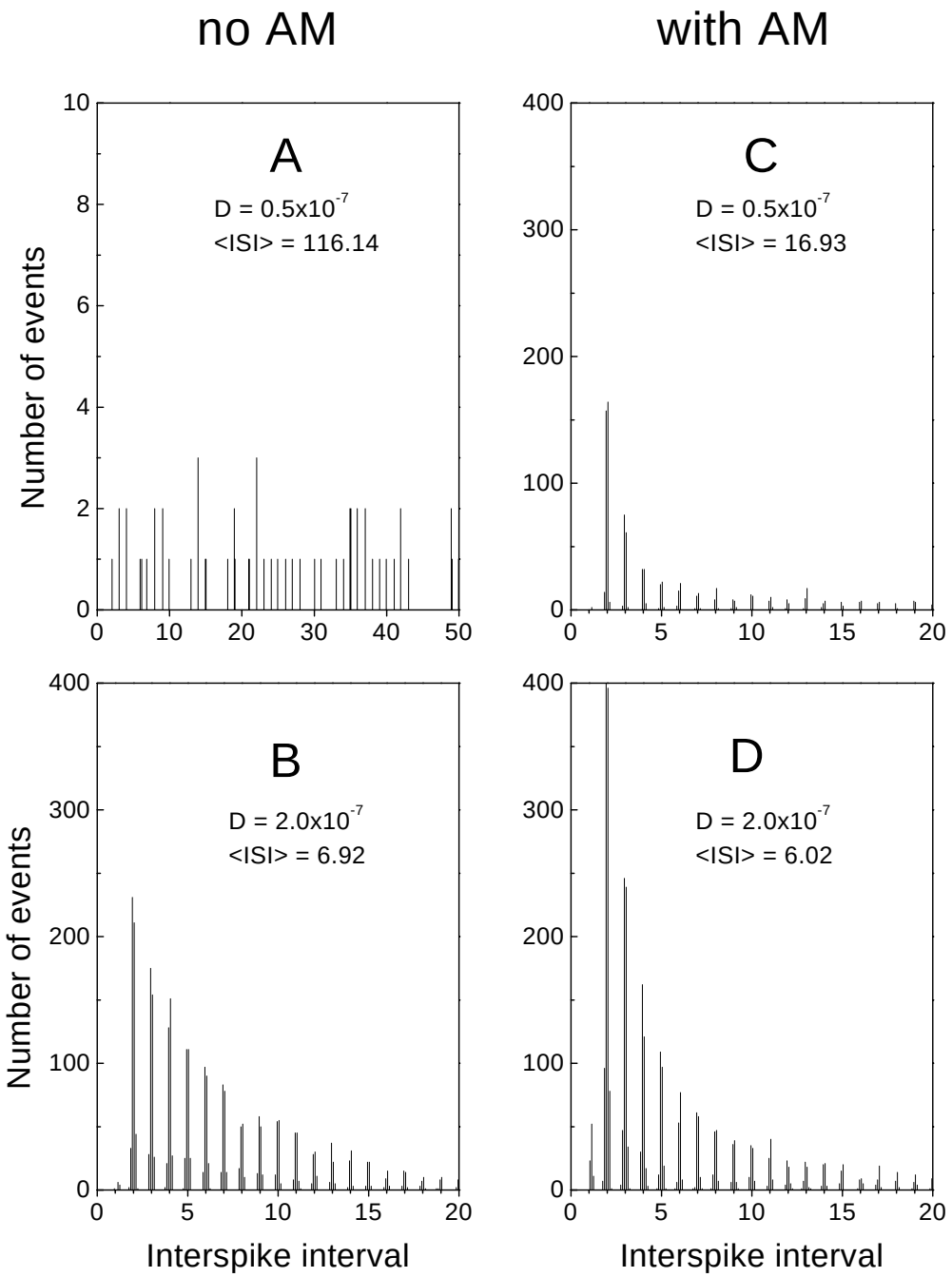

Fig. 6. Interspike interval histograms in the subthreshold regime ($r = 0.01$) for two internal noise intensities, (left panels) without and (right panels) with amplitude modulation (AM). Parameter values are given in the insets. The interspike intervals are given in units of the carrier period. Histograms were constructed from 2×10^7 integration time steps of 0.001 s, thus corresponding to 20 000 s (the first 100 s were discarded as transients). Note that the scales of histogram A were changed due to very few events in the region considered. The EOD carrier frequency is 1 Hz.

a maximum. For larger D, spikes start occurring more randomly, i.e. at irrelevant times, and the coding fraction decreases. This is a form of stochastic resonance [Gammaitoni *et al.*, 1998; Collins *et al.*, 1995; Chialvo *et al.*, 1997]. The novelty here is that the forcing is done with an amplitude-modulated carrier, the AM's time scale being longer than the carrier period.

As the mean carrier amplitude gets closer to threshold (12.8 for $T = 1$), the noise amplitude that maximizes the coding fraction becomes smaller, as is seen in Fig. 9. This occurs because less noise

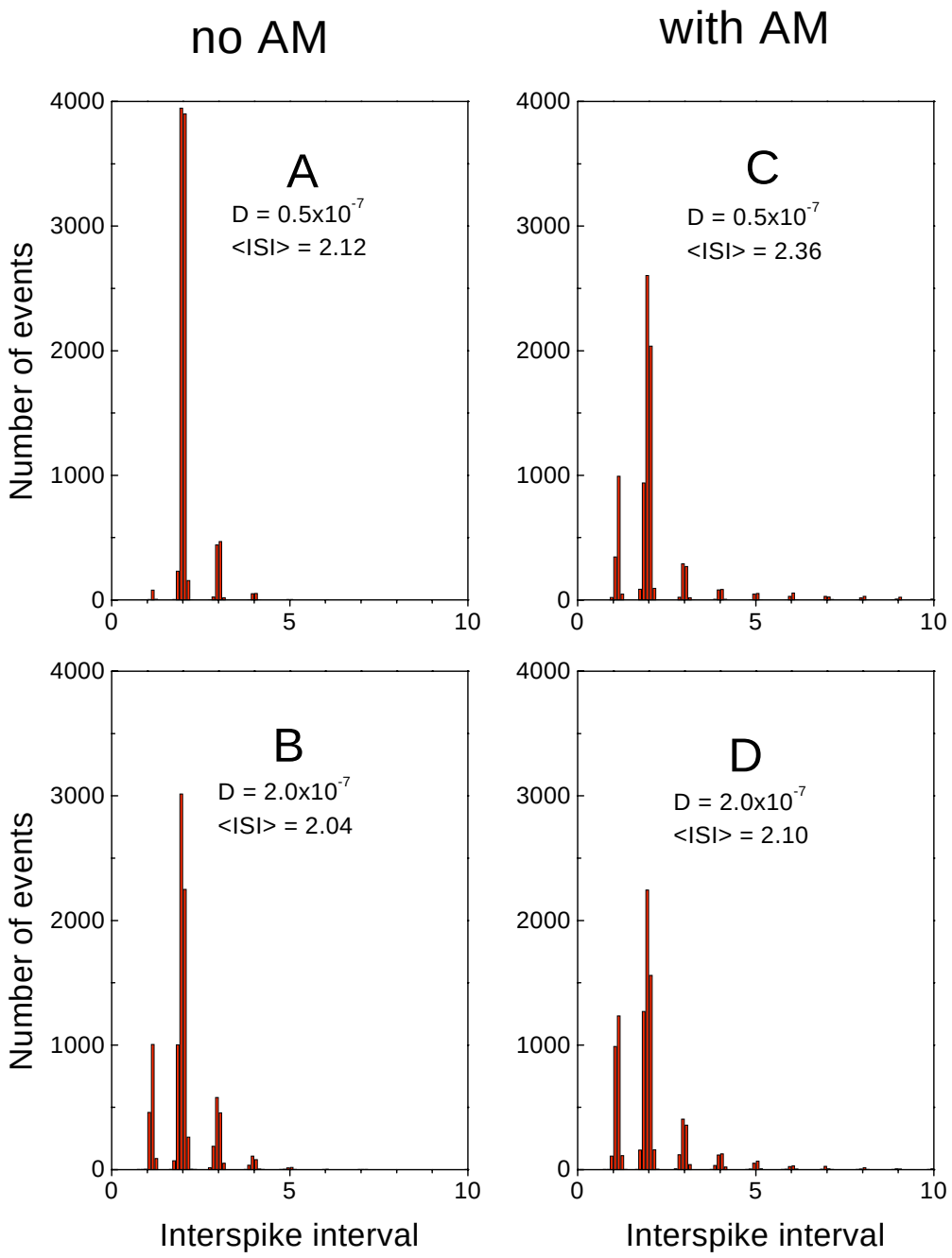

Fig. 7. Interspike intervals histograms (constructed as in Fig. 8) in the supratreshold regime ($r = 0.014$) for two internal noise intensities, (left panels) without and (right panels) with amplitude modulation (AM). The interspike intervals are given in units of the carrier period. The EOD carrier frequency is 1 Hz.

is now needed to significantly increase spiking, due to the reduced effective barrier height. Figure 9 also shows that γ is proportional to r for values of r well into the suprathreshold regime, but not for $r > 0.018$.

Figure 10 presents preliminary results on the effect of the EOD frequency on the coding fraction. The same noise realization was used for each value of EOD frequency, and was the same as that used for Figs. 8 and 9. This implies that the actual physical time of the physical random AM stimulus was also the same in each case. Also, all other parameters of the simulations were held fixed, the stimulus amplitude was $r = 0.011$, a value in the subthreshold regime, and the noise intensity was set to $D = 8 \times 10^{-8}$. This value of D yields the

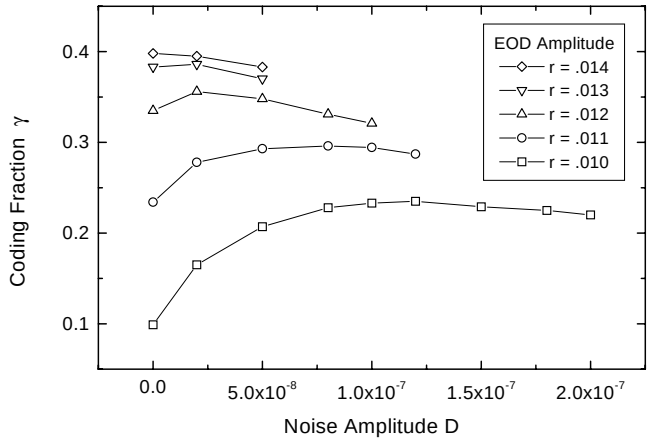

Fig. 8. Coding fraction as a function of internal noise intensity D for different mean amplitudes of the carrier, spanning the range from below to above threshold. Each curve represents a fixed mean carrier amplitude around which $s(t)$ fluctuates with constant contrast (same ratio between the amplitude r and the standard deviation of $s(t)$). In the subthreshold regime, and in the suprathreshold regime near threshold, internal noise enhances the transfer of information about carrier amplitude modulations to the output spike train. For each parameter combination, the coding fraction was estimated using one spike train obtained from 20 000 s of simulated spike trains, i.e. from 2×10^7 integration time steps of 0.001 s (the first 10^5 time steps were discarded as transients). The coding fraction is obtained first by computing the optimal filter $h(t)$. This is done using spectral estimates that are averaged over consecutive 512 s windows. This filter is then convolved with the whole spike train; the error and coding fractions are then computed. The EOD carrier frequency is 1 Hz.

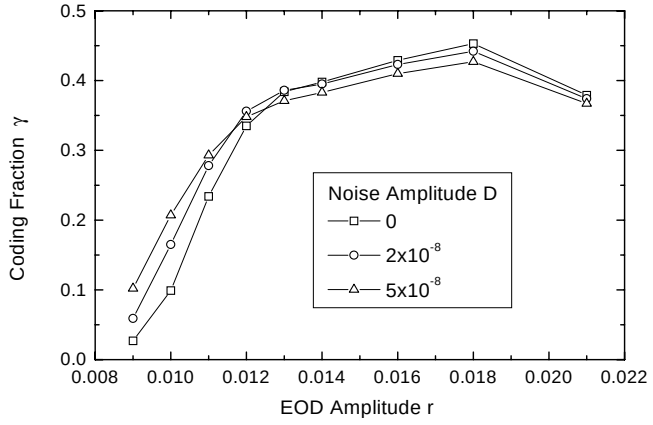

Fig. 9. Influence of mean carrier amplitude on information transfer. The coding fraction, calculated as in Fig. 8, is plotted as a function of amplitude r for different internal noise intensities. The mean amplitude modulation is as in Fig. 4. Note the crossover in the ordering of the curves in the vicinity of threshold $r = 0.0128$. The carrier frequency is 1.0 Hz. Note that all simulations are done at constant contrast, i.e. constant ratio of standard deviation of the modulation to the mean carrier amplitude.

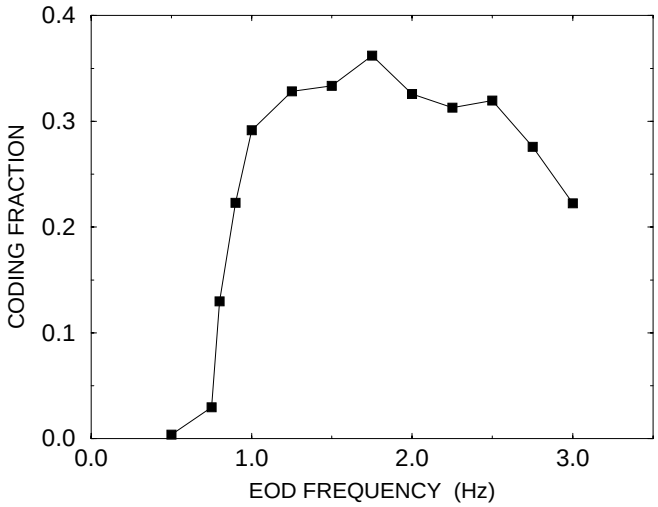

Fig. 10. Effect of the EOD frequency Ω on the coding fraction. The EOD amplitude in the absence of AM's is $r = 0.011$, and the internal noise intensity is $D = 8 \times 10^{-8}$. The same realization for the "random" amplitude modulation was used in each case, and this was the same as that used in Fig. 8. Coding fractions were computed as in Fig. 8.

maximum coding fraction for this value of r (see Fig. 8).

The coding fraction is seen to go through a maximum as a function of EOD frequency. This can be explained as follows, based on our knowledge [Longtin, 2000] of the tuning curves of the FHN model for these parameters, and their modification by noise. The left part of Fig. 10 corresponds to higher forcing periods; at these periods, the deterministic dynamics are subthreshold. Thus, for the small noise used here, there is very little firing, and even less as the forcing period increases. This causes the coding fraction to be low.

The shape of the 2:1 boundary in the amplitude-forcing period subspace [Longtin, 2000] is roughly a horizontal line over the region where the coding fraction is around 0.3 in Fig. 10; its shape is not altered much by internal noise of the magnitude used here. In other words, over the approximate range of EOD frequencies $(1.0, 2.5)$ Hz, the firing in the absence of AM's and of internal noise follows a 2:1 pattern that varies little with EOD frequency; adding a small amount of internal noise does not alter this pattern much either. Thus, the coding fraction is not expected to vary much over this range of EOD frequencies, as Fig. 10 reconfirms. However, beyond an EOD frequency of 2.5 Hz, the deterministic pattern has less spikes per unit time (such as a 3:1 pattern), i.e. a smaller firing rate. With internal noise, the coding fraction drops accordingly.

Further analysis of this dependence of the coding fraction on the EOD frequency, and its implications for the tuning of electroreceptors to the EOD, will be discussed in greater detail elsewhere.

5. Coding AM's from the Suprathreshold Regime

5.1. *Deterministic case*

In the suprathreshold regime without internal noise but with AM's, there are many firings whenever the AM's bring the voltage above threshold, as shown in Fig. 5. Note that without AM's, there is continuous firing at a constant frequency (2:1); segments of such patterns are visible in Fig. 5B. Decreases in the carrier amplitude interrupt this relatively constant firing rather abruptly; this is a consequence of the behavior of the firing frequency near a Hopf bifurcation. It is interesting to note that, in this noiseless case, the AM by itself (i.e. without internal noise) can generate a multimodal ISIH as seen in Fig. 1D. This is true even though the carrier alone (without AM's) generates a periodic firing pattern, thus a singular ISIH with only one peak. It is also the case that the lower parts of the AM fluctuations are not encoded by spikes, because they are subthreshold.

5.2. *Stochastic case*

In the suprathreshold case with AM's, the effect of noise on the mean firing rate depends on the intensity D. At low D, the mean firing rate actually decreases when AM's are present (see also Fig. 3). Negative AM fluctuations deleted spikes from an otherwise almost periodic pattern; in other words, the small internal noise slightly disturbs the periodically firing solution above the Hopf bifurcation, and negative AM fluctuations delete spikes from this pattern. The effect of internal noise and AM's on the ISIH's is shown in Fig. 7. The mean intervals printed in the insets show that the AM's decrease the firing rate. This was anticipated in Fig. 3 at low noise. For mid to high noise, the AM makes little difference on the mean firing rate. However, with or without AM's, increasing the internal noise D increases the firing rate, a consequence of the Arrhenius factor and its modification by small signals [Gammaitoni *et al.*, 1998; Longtin, 2000].

5.3. *Coding fraction*

Just above threshold, for $r = 0.013$, it is seen from Fig. 8 that the internal noise still increases the coding fraction, although very slightly. At higher values of r, the randomizing effect of the internal noise is found to always decrease the coding fraction. Thus, stochastic resonance does not occur at these mean carrier amplitudes. The best reconstruction of the signal using the spike train and the optimal filter computed as described in Sec. 2 is obtained for the pure deterministic dynamics of the FHN model considered here. Other measures such as mutual information are currently being investigated to determine the effect of noise from a more general perspective than linear theory. We note in both the sub- and suprathreshold cases that the plateaus in the γ versus D plots are fairly long and flat. Thus, one could say that the internal noise causes rather small changes in coding fraction in the suprathreshold case. Of course, the changes in γ are drastic before the maximum in the subthreshold case.

6. Discussion

We have presented a study of possible origins of a certain kind of random firing pattern using a periodically forced excitable system (the FitzHugh–Nagumo system), and of the modification of this pattern by internal quasi-white noise and random bandlimited modulations of the amplitude of the forcing. We have focussed on experimentally observed patterns for which the interspike interval histograms (ISIH) are multimodal with smooth peaks centered at integer multiples of the forcing period, and for which the envelope of this ISIH is unimodal (i.e. has one maximum). We have discussed how stochastic phase locking due to noise, or to subthreshold chaos plus noise, can underlie such firing patterns. We have shown the effect of noise on certain simple synchronization properties of these dynamics, and their modification by amplitude modulation and internal noise.

The phase locking pattern itself is fairly robust to 15% modulation, as no qualitative changes are observed; only the mean firing frequency changes, in a manner dependent on the noise level and on whether the dynamics are sub- or suprathreshold without AM's. The coding fraction was also used to quantify the locking of spikes to slow amplitude modulations of the carrier, i.e. to quantify how well

the spike train represents the signal. This is a different question than that of quantifying the behavior of a phase difference between system and input — a question that could be studied using e.g. analytical signal theory [Neiman *et al.*, 1999]. We also find that the coding fraction increases monotonically with mean carrier amplitude.

We find that internal noise can increase the coding fraction in the subthreshold case, all the while preserving the phase locking to the underlying carrier. Thus, this internal noise could be used to transfer information about slow AM's, while preserving fine temporal code on the time scale of the carrier period. This is similar to studies of rate coding in noisy neurons [Knight, 1972], and in particular to studies of aperiodic SR [Collins *et al.*, 1995; Levin & Miller, 1996]. One difference here however is that we are not directly applying the signal to the voltage dynamics: It is applied to the amplitude of a periodic signal which drives dv/dt. Hence, although rate coding is apparent, all firings are still precisely phase locked to an underlying high frequency forcing. There is thus a precisely timed component to the rate coding of the AM's on a slower time scale (the ratio of the carrier frequency to the cutoff frequency for the AM's in Fig. 10 is $2\pi/\alpha = 4\pi$, which is in the physiological range). More extensive results, in particular on the ability of the FHN system (and other more accurate models) to transmit information about carrier AM's depending on various parameters, are forthcoming.

It is striking that the voltage response to AM's mirrors quite well the AM itself (when there are no spikes — this is most obvious in the subthreshold regime, e.g. Fig. 4A). The AM appears to simply be superimposed on a background depolarization of mean value proportional to the carrier amplitude. This is a consequence of the fact that the spikes are strongly phase locked to the carrier. One could attempt a theory of the effects reported here by first replacing the carrier by an additional bias current I that sets the mean voltage (resting potential) at a value corresponding to that produced by the carrier maximum. Then, one could simply add the noisy signal $s(t)$, and see if the coding fraction is the same as in Figs. 8 and 9. However, this approach does not work. In particular, even the basic mean firing rates cannot be reproduced by replacing the carrier by a bias. Since the coding fraction is quite sensitive to the firing rate, this yields quite different results for γ versus D.

We come back to one point mentioned in Sec. 5: AM's can generate multimodal ISIH even without internal noise in the suprathreshold case. This is true also in the subthreshold case, although the firings are rare. Why then include noise in the modeling of such cells? The answer to this is simple: If the AM is turned off, the ISIH is singular (only one peak at $2T$ in our example), while the experimental ISIH's have ISIH's as in Fig. 1. Thus, to better represent the biological situation, our study suggests that some internal noise is required to first produce a proper skipping response which results from the kind of stochastic phase synchronization studied in our paper. Then, the effect of the AM is to shift the probability of firing per forcing cycle, with the variations in firing rate and ISIH shown, respectively, in Figs. 2 and 3, and 6 and 7.

The carrier frequency was kept constant throughout our work, except for Fig. 10 where it was varied while keeping the EOD amplitude and internal noise intensity constant. The coding fraction exhibits a maximum as a function of this EOD frequency, for the reasons suggested at the end of Sec. 4.3 which involve the tuning characteristic of the FHN oscillator [Longtin, 2000; Hochmair-Desoyer *et al.*, 1984]. It would certainly be worthwhile investigating more closely the connection between the coding fraction and the tuning curves of the system. We expect that, generally, carrier frequencies close to the preferred frequency of the excitable system will produce the highest coding fractions.

It is clear from our results that biophysical noise in the neuron and its synapses can, under certain circumstances, enhance the transfer of information about AM's to output spike trains. This happens in the subthreshold regime. In fact, because the AM is a Gaussian bandlimited noise, there always is a finite firing probability when $D_2 > 0$. The issue of how the firing statistics without AM's are determined by combinations of stimulus amplitude, frequency and synaptic noise intensity (to name the more important parameters), and how these combinations compare in terms of their coding fractions, will be explored in a subsequent paper.

Relatedly, it is important to note that we have used a sinusoidal forcing signal throughout our work. For many systems, stimuli are half-wave rectified before exerting their forcing on the equations governing excitability (see e.g. [Gabbiani, 1996]). Such rectification is performed by a specialized

receptor or transducer that is sensitive only to one polarity of the forcing, or to the derivative of the forcing. Such rectified sinusoidal input also approximates pulsatile forcing of nerve [Rattay, 1990] when the duty cycle of the forcing is close to 50%. For the frequency used in our study, preliminary results (not shown) indicate that this rectification produces minor quantitative differences with the results presented here. In particular, the voltage response to the rectified version of the carrier produces an undershoot when the stimulus goes negative; thus, the resulting waveform does not differ significantly from that obtained with the full sinusoid. Also, since the main difference between the two waveforms occurs on the portions of the response furthest from threshold, there are only minor differences between the resulting firing patterns. This will be detailed elsewhere.

Acknowledgments

This work was supported by NSERC Canada. We are grateful to Maurice Chacron, Lutz Schimansky-Geier, Jan Freund and Len Maler for useful discussions.

References

Alexander, J. C., Doedel, E. J. & Othmer, H. G. [1990] "On the resonance structure in a forced excitable system," *SIAM J. Appl. Math.* **50**, 1373–1418.

Brown, D., Feng, J. & Feerick, S. [1999] "Variability of firing of Hodgkin–Huxley and FitzHugh–Nagumo neurons with stochastic input," *Phys. Rev. Lett.* **82**, 4731–4734.

Chialvo, D., Longtin, A. & Müller-Gerking, J. [1997] "Stochastic resonance in models of neuronal ensembles," *Phys. Rev.* **E55**, 1798–1808.

Clay, J. R. [1976] "A stochastic analysis of the graded response of nerve membrane," *J. Theor. Biol.* **59**, 141–158.

Clay, J. R. & Shrier, A. [1999] "On the role of subthreshold dynamics in neuronal signaling," *J. Theor. Biol.* **197**, 207–216.

Collins, J. J., Chow, C. C. & Imhoff, T. [1995] "Aperiodic stochastic resonance," *Phys. Rev.* **E52**, R3321–3324.

Gabbiani, F. [1996] "Coding of time-varying signals in spike trains of linear and half-wave rectifying neurons," *Network: Comput. Neural Syst.* **7**, 61–85.

Gammaitoni, L., Hänggi, P., Jung, P. & Marchesoni, F. [1998] "Stochastic resonance," *Rev. Mod. Phys.* **70**, 223–287.

Gerstner, W., van Hemmen, J. L. & Cowan, J. D. [1996] "What matters in neuronal locking?" *Neural Comput.* **8**, 1653–1676.

Glass, L. & Mackey, M. C. [1988] *From Clocks to Chaos. The Rhythms of Life* (Princeton University Press, Princeton, NJ).

Hochmair-Desoyer, I. J., Hochmair, E. S., Motz, H. & Rattay, F. [1984] "A model for the electrostimulation of the nervous acusticus," *Neuroscience* **13**, 553–562.

Johnson, D. H. [1996] "Point process models of single-neuron discharges," *J. Comput. Neurosci.* **3**, 275–299.

Kaplan, D. T., Clay, J. R., Manning, T., Glass, L., Guevara, M. R. & Shrier, A. [1996] "Subthreshold dynamics in periodically stimulated squid giant axons," *Phys. Rev. Lett.* **76**, 4074–4077.

Knight, B. [1972] "Dynamics of encoding in a population of neurons," *J. Gen. Physiol.* **59**, 734–766.

Kurrer, C. & Schulten, K. [1995] "Noise-induced synchronous neuronal oscillations," *Phys. Rev.* **E51**, 6213–6218.

Levin, J. E. & Miller, J. P. [1996] "Broadband neural encoding in the cricket cercal sensory system enhanced by stochastic resonance," *Nature* **380**, p. 165.

Lewis, E. R. & Henry, K. R. [1995] "Nonlinear effects of noise on phase-locked cochlear nerve responses to sinusoidal stimuli," *Hearing Res.* **84**, 72–80.

Lindner, B. & Schimansky-Geier, L. [1999] "Analytical approach to the stochastic FitzHugh–Nagumo system and coherence resonance," *Phys. Rev.* **E60**, 7270–7276.

Longtin, A. [1993] "Stochastic resonance in neuron models," *J. Stat. Phys.* **70**, 309–327.

Longtin, A. & Racicot, D. M. [1997] "Spike train patterning and forecastability," *Biosystems* **40**, 111–118.

Longtin, A. [1998] "Firing dynamics of electroreceptors," *Int. Conf. Neural Information Processing ICONIP'98*, KitaKyushu City, Japan, October 1998, pp. 27–30.

Longtin, A. & Chialvo, D. [1998] "Stochatic and deterministic resonances in excitable systems," *Phys. Rev. Lett.* **81**, 4012–4015.

Longtin, A. [2000] "Effect of noise on the tuning properties of excitable systems," *Chaos Solit. Fract.* **11**, 1835–1848.

Motz, H. & Rattay, F. [1986] "Study of the application of the Hodgkin–Huxley and the Frankenhaeuser–Huxley model for the electrostimulation of the acoustic nerve," *Neuroscience* **18**, 699–712.

Neiman, A., Silchenko, A., Anishchenko, V. & Schimansky-Geier, L. [1998] "Stochastic resonance: Noise-enhanced phase coherence," *Phys. Rev.* **E70**, 7118–7125.

Neiman, A., Schimansky-Geier, L., Moss, F., Shulgin, B. & Collins, J. J. [1999] "Synchronization of noisy systems by stochastic signals," *Phys. Rev.* **E60**, 284–292.

Nelson, M. E., Xu, Z. & Payne, J. R. [1997] "Characterization and modeling of P-type electrosensory afferent responses to amplitude modulations in a wave-type electric fish," *J. Comp. Physiol.* **A181**, 532–544.

Pikovsky, A. S. & Kurths, J. [1997] "Coherence resonance in a noise-driven excitable system," *Phys. Rev. Lett.* **78**, 775–778.

Pikovsky, A., Rosenblum, M. G., Osipov, G. V. & Kurths, J. [1997] "Phase synchronization of chaotic oscillators by external driving," *Physica* **D104**, 219–238.

Rattay, F. [1990] *Electrical Nerve Stimulation. Theory, Experiments, and Applications* (Springer-Verlag, Wien).

Rescigno, A., Stein, R. B., Purple, R. L. & Poppele, R. E. [1970] "A neuronal model for the discharge patterns produced by cyclic inputs," *Bull. Math. Biophys.* **32**, 337–353.

Rieke, F., Warland, D., de Ruyter van Steveninck, R. & Bialek, W. [1997] *Spikes* (MIT press, Cambridge, MA).

Rose, J., Brugge, J., Anderson, D. & Hind, J. [1967] "Phase-locked response to low-frequency tones in single auditory nerve fibers of the squirrel monkey," *J. Neurophysiol.* **30**, 769–793.

Scheich, H., Bullock, T. H. & Hamstra, R. H. Jr. [1973] "Coding properties of two classes of afferent nerve fibers: High-frequency electroreceptors in the electric fish, *Eigenmannia*," *J. Neurophysiol.* **36**, p. 39.

Segundo, J. P., Vibert, J. F., Pakdaman, K., Stiber, M. & Diez Martinez, O. [1994] "Noise and the neurosciences; A long history, a recent revival, and some theory," in *Origins: Brain and Self Organization*, ed. Pribram, K. (Lawrence Erlbaum Associates, Hillsdale, NJ).

Theunissen, F. & Miller, J. P. [1995] "Temporal encoding in nervous systems: A rigorous definition," *J. Comput. Neurosci.* **2**, 149–162.

Treutlein, H. & Schulten, K. [1985] "Noise induced limit cycles of the Bonhoeffer–van der Pol model of neural pulses," *Ber. Bunsenges. Phys. Chem.* **89**, p. 710.

Tuckwell, H. C. & Rodriguez, R. [1998] "Analytical and simulation results for stochastic Fitzhugh–Nagumo neurons and neural networks," *J. Comput. Neurosci.* **5**, 91–113.

Wessel, R., Koch, C. & Gabbiani, F. [1996] "Coding of time-varying electric field amplitude modulations in a wave-type electric fish," *J. Neurophysiol.* **75**, 2280–2293.

Xu, Z., Payne, J. R. & Nelson, M. E. [1996] "Logarithmic time course of sensory adaptation in electrosensory afferent nerve fibers in a weakly electric fish," *J. Neurophysiol.* **76**, 2020–2032.

Zakon, H. H. [1986] "The electroreceptive periphery," *Electroreception*, eds. Bullock, T. H. & Heiligenberg, W. (Wiley-Interscience, NY), pp. 103–156.